

Toward Apparent Negative Permittivity Measurement in a Magnetic Nanofluid with Electrically Induced Clusters

Michal Rajnak,^{1,2,*} Zdenko Spitalsky,³ Bystrík Dolník,² Juraj Kurimsky,² Ladislav Tomco,⁴ Roman Cimbala,² Peter Kopecký,¹ and Milan Timko¹

¹*Institute of Experimental Physics SAS, Watsonova 47, 04001 Košice, Slovakia*

²*Faculty of Electrical Engineering and Informatics, Technical University of Košice, Letná 9, 04200 Košice, Slovakia*

³*Polymer Institute SAS, Dúbravská cesta 9, 845 41 Bratislava, Slovakia*

⁴*Faculty of Aeronautics, Technical University of Košice, Rampová 7, 04121 Košice, Slovakia*

(Received 30 September 2018; revised manuscript received 3 December 2018; published 12 February 2019)

It is known that the permittivity of a magnetic nanofluid is controllable by external magnetic fields. The resulting effect of magneto-dielectric anisotropy originates in the magnetic nanoparticle assembly formation induced by the applied magnetic field. The particle assembly in magnetic nanofluids can be induced even by a dc electric field. Then, analogous to the magneto-dielectric effect, a question arises concerning the effect of the dc bias electric field on the nanofluid permittivity in a wide frequency range. We present dielectric spectra (1 mHz–1 MHz) measured on a transformer oil-based magnetic nanofluid at various temperatures. Electrode polarization and an interfacial relaxation process are analyzed. We show that the applied dc bias voltage results in permittivity sign switching at low frequencies. The critical frequency at which the sign is reversed depends on the nanofluid temperature and the dc bias voltage level. The nanoparticle assembly and conductive percolative paths are considered as key mechanisms leading to the transition from capacitive to inductive reactance. The measurement of apparent negative permittivity in a dc electric field can be used as a simple method for the detection of electric field-induced particle assembly and percolation. The permittivity sign control by means of a dc bias voltage may open an alternative avenue for research and applications of magnetic nanofluids.

DOI: 10.1103/PhysRevApplied.11.024032

I. INTRODUCTION

The development of nanodielectrics has gained remarkable scientific attention since an appreciation of unique conductive and dielectric properties of interfaces was realized [1–3]. Extensive research has shown that the addition of just a few weight percent of nanofillers in polymers has a profound impact on their physical, chemical, mechanical, and electrical properties [4]. From a dielectric and electrical insulation point of view, the top priority has been focused on the breakdown strength of the polymers. It was shown that nanofillers increase the dielectric breakdown strength and the resistance against partial discharge and treeing in polymers [5,6]. A similar approach has been applied to the modification of standard dielectric and insulating liquids, mostly represented by various mineral oils [7]. In this way, nanofluids for electrical engineering applications were developed by dispersing suitable nanosized particles (from 1 to 100 nm) in the carrier liquid [8–11]. A number of experimental studies reported

the enhanced heat transfer [12–14] and insulating properties [15–17] of the insulating nanofluids.

Special attention has been paid to magnetic nanofluids (ferrofluids). They are colloidal suspensions of magnetic nanoparticles (MNP) in a liquid carrier [18]. Those based on transformer oils constitute an attractive cooling and insulating medium for electrical power apparatus. In addition to the enhanced thermal conductivity, the cooling by magnetic nanofluid (MNF) relies on thermomagnetic convection [19–21]. On the other hand, the dispersed MNP can increase the electric breakdown field strength of transformer oils [22–24]. This phenomenon is probably associated with charge trapping on the nanoparticles and the resulting streamer propagation velocity reduction, as recently simulated [25,26]. Moreover, it is well known that the relative permittivity of nanofluids is strongly dependent on the nanoparticle material, shape, and volume fraction [15,27]. In addition, the permittivity of MNF is controllable by external magnetic fields. The related effect of magneto-dielectric anisotropy [28,29] originates in the MNP assembly formation induced by the applied magnetic field. Recently, it was shown that the particle assembly in MNF can even be induced by an electric

*rajnak@saske.sk

field [30–33]. However, the assembly formation is feasible only with dc or low-frequency electric fields [31]. In this case, the dielectric contrast between the nanoparticles and the carrier liquid and the resulting effective nanoparticle polarization play key roles. Then, analogous to the magneto-dielectric effect, a question arises concerning the effect of the dc bias electric field on the nanofluid permittivity measured at various frequencies of an ac electric field.

A dielectric spectrum of MNF based on transformer oil measured above 20 Hz may exhibit a dielectric relaxation shift to lower frequencies upon application of a dc bias electric field [30]. However, the permittivity below 20 Hz down to 1 mHz with the superimposed dc bias field has not yet been closely documented. This is the frequency range where the structural changes take place [31]. It was shown that electrorheological fluids can exhibit permittivity sign switching (from positive to negative) at low frequencies as a result of a dc bias electric field [34,35]. In this case, the collective behavior of the field-induced particle aggregates is proposed to account for the negative permittivity (NP). In literature, the NP of nanofluids at low frequencies has rarely been reported. On the contrary, in materials like Schottky diodes [36] and fuel cells [37], the low-frequency NP was considered as a local electrochemical effect or a thermally induced charge detrapping. In metal-semiconductor structures, the NP at low frequencies and bias voltages was attributed to interfacial polarization, interface traps, and series resistance [38]. The effect of NP at low frequencies was also observed in polypropylene carbon nanotube nanocomposites [39], polyaniline magnetite nanocomposites [40], and polyaniline nanocomposites with different carbon nanostructures [41]. Recently, it was shown that negative capacitances can be obtained in bilayer capacitors by applying a dc bias electric field [42]. Indeed, negative capacitance materials are gaining greater interest as the serial connection of negative capacitance and positive capacitance, in principle, can result in an unlimited capacitance density [43]. On the other hand, there are well-known composite media with simultaneous negative permeability and permittivity in the microwave regime [44]. Tunable NP in radio and microwave frequencies was observed in percolative Fe/Al₂O₃ composites [45] and silver yttrium iron garnet materials [46]. These materials have the potential to be used as electromagnetic wave absorbers, shields, and antennas. NP and resonances are observable in single-negative plasmonic metamaterials such as yttrium iron garnet [47] and yttrium barium copper oxide superconductors [48]. Furthermore, various nanostructured metamaterials with a negative refractive index are also well known [49].

Here, we report on the apparent NP of transformer oil-based MNF induced by the application of a dc bias electric field. We present a broadband dielectric spectrum of the MNF, which exhibits negative values at low frequencies

after the application of the dc bias voltage on the measuring capacitor. We describe the conditions leading to the observed phenomenon and provide a potential interpretation. Based on the observed effect, we propose its utilization in the study of self-assembly and some other applications of MNF in the field of electrical engineering.

II. MATERIALS AND METHODS

The MNF investigated in this study is based on a commercial transformer insulating oil (the viscosity at 40 °C is 11 mm²/s and the relative density is 870 kg/m³). The dispersive phase consists of iron oxide nanoparticles synthesized by chemical coprecipitation and stabilized with oleic acid adsorbed onto the MNP surfaces. The mean area-equivalent particle core diameter (without the surfactant shell) is found to be 10.55 nm, as determined by transmission electron microscopy and subsequent number-based particle size distribution with a standard deviation of 2.17 nm. In the studied MNF, the magnetic particle volume fraction is 6.6%. The preparation procedure and basic physical characterization have been published elsewhere [30,50].

In order to study the influence of cooperative phenomena such as electrically induced particle ordering on the MNF dielectric response, the method of dielectric spectroscopy is employed. The complex dielectric permittivity is measured by a Novocontrol broadband dielectric spectrometer (Concept 40) utilizing the Alpha-A modular measurement system. To obtain a full picture of the relaxation phenomena expected in the MNF, the experiments are performed at frequencies ranging from 1 mHz up to the MHz region. The sample (2.5 ml) is poured in a liquid sample cell with concentric cylindrical electrodes (3.4-mm gap) and a guard ring (Novocontrol). This geometry avoids errors related to the thermal expansion of a measured liquid and protects against sample leakage. It also increases the accuracy of the measurement by decreasing the influence of fringing fields. The electrodes are fed with the effective testing voltage of 1 V biased with a dc voltage up to 40 V. Taking into account the various ambient and transformer operating conditions and to reveal the relaxation dynamics, the dielectric spectra are collected at temperatures from 233 to 383 K. To verify the reproducibility of the experimental results, an independent *LCR* meter (IM3533 HIOKI) is used as a complementary device. The data are treated by OriginLab software.

As the MNF (transformer oil) is expected to undergo a liquid-solid phase transition in the given temperature range, we employ temperature-dependent magnetometry as a complementary method to reveal the phase transition. The MNF magnetization (40- μ l sample volume) is measured by means of a vibrating sample magnetometer (VSM) installed on a superconducting magnet from Cryogenic Limited. The measurements are performed in zero

field cooling (ZFC) and field cooling (FC) regimes in the available temperature range from 2 to 300 K.

To get a better view of the dc electric current in the MNF, which can possibly lead to the apparent NP, the current-voltage characteristics and the time dependence are measured by model 6517B electrometer/high-resistance test and measurement system (Keithley, USA). As an electrode system, we use a glass plate capacitor (liquid-crystal cell) with Indium Tin Oxide (ITO) electrodes separated by 50 μm . Within these measurements, the voltage is continuously changed with 10-V steps in the range from -50 to 50 V. Each particular voltage value is held for a period of 8 min during which the current is measured.

III. RESULTS AND DISCUSSION

The dielectric response of the pure transformer oil in the form of the complex permittivity is presented in Figs. 1(a)–1(c). One can see that the real permittivity [Fig. 1(a)] exhibits frequency- and temperature-independent behaviors at frequencies above 0.1 Hz. The measured values in the presented spectra are close to 2, which represents a typical relative permittivity of transformer oils. Below 0.1 Hz, a steep increase in the real permittivity with decreasing frequency is observed. This behavior is most pronounced at the highest temperature, while the effect diminishes with decreasing temperature. Similarly, the increase is observed in the imaginary permittivity and the dissipation factor (known as $\tan \delta$), which is defined as the ratio of the imaginary and real parts of the complex permittivity. Thus, the simultaneous low-frequency increase in the real permittivity and dielectric loss is a typical manifestation of the electrode polarization. This well-known phenomenon arises due to the charge accumulation and formation of interfacial layers of reduced mobility at the contacts with the metal electrodes. In this case, the free charge is represented by various additives, which, in connection with water (moisture) as the most prominent impurity in transformer oils, constitute the main source of the free charge.

The shift of the electrode polarization onset to higher frequencies with increasing temperature is qualitatively in concurrence with a theoretical model [51], where the characteristic polarization time τ_{EP} is determined as follows:

$$\tau_{EP} = \frac{d}{2\mu} \left(\frac{\varepsilon_R \varepsilon_0}{p_0 k T} \right)^{1/2}. \quad (1)$$

In Eq. (1), d is the electrode separation distance, ε_0 is the permittivity of free space, p_0 is the equilibrium number density of free charges with mobility μ , k is Boltzmann's constant, and T is the absolute temperature. In addition to the electrode polarization effect, the free charge also contributes to the electrical dc conductivity σ as $\varepsilon'' \approx$

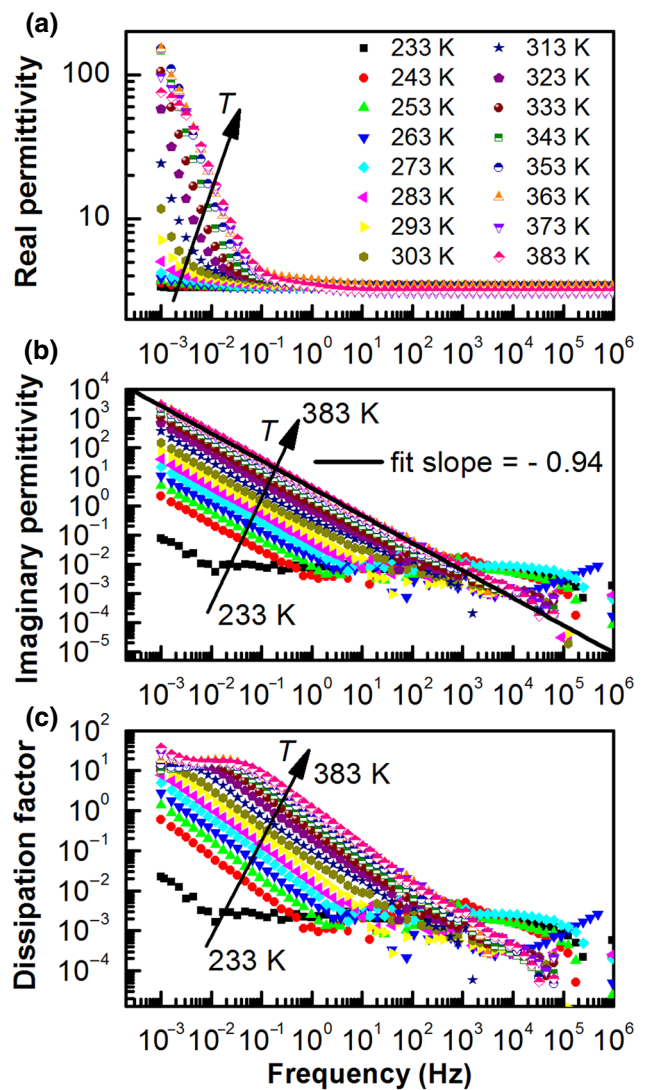


FIG. 1. The dielectric spectra measured on the transformer oil at various temperatures. (a) Real part of the complex permittivity, (b) imaginary part of the complex permittivity, and (c) dissipation factor.

$\sigma/2\pi f$. This is determined from the observed imaginary permittivity slope in the frequency regions, where the real permittivity exhibits constant behavior. Fitting the imaginary permittivity spectra with a power law yields the slope value -0.94 , which is greater than -1 , thus indicating the conductivity contribution.

The dielectric spectrum of the studied MNF at various temperatures is depicted in Fig. 2. At temperatures from 383 to 253 K, the real permittivity [Fig. 2(a)] exhibits a steep increase with decreasing frequency (below 100 Hz). This dielectric dispersion tends to saturate at lower frequencies and reaches colossal permittivity values. Clearly, this behavior is accompanied by increasing imaginary permittivity with decreasing frequency [Fig. 2(c)] and a remarkable maximum in the dissipation factor spectrum

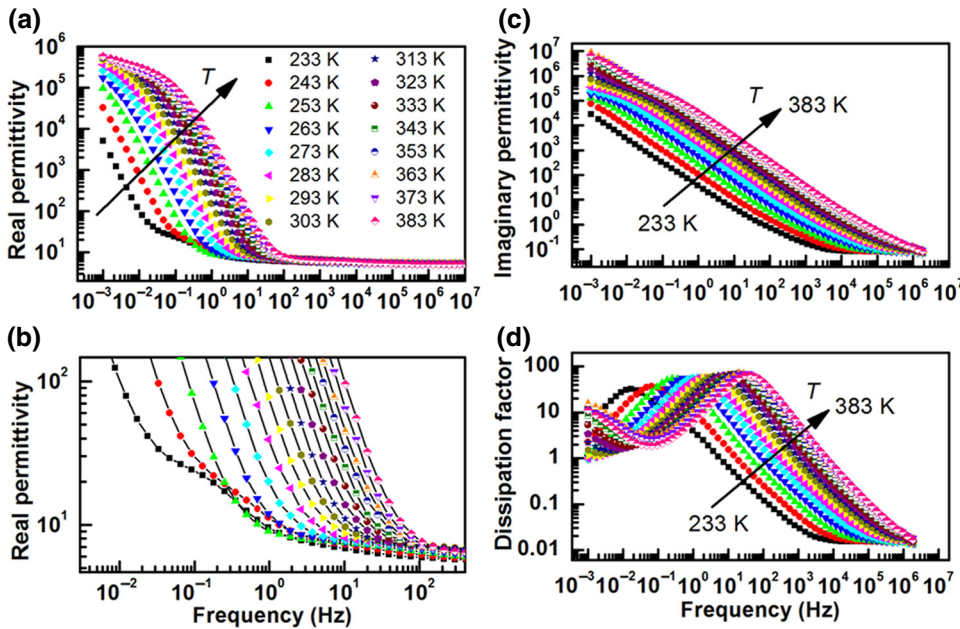


FIG. 2. The real permittivity spectrum of the magnetic nanofluid at various temperatures (a) with the enlarged view focused on the dispersion at lower temperatures (b). The dielectric loss is presented in the form of imaginary permittivity (c) and dissipation factor spectrum (d).

[Fig. 2(d)]. Analogous to the behavior in the transformer oil, one can consider this dispersion as a pronounced electrode-polarization effect due to nanoparticle blocking. However, taking into account Eq. (1), the migrating nanoparticles with considerably lower mobility than that of the free charge in the oil will cause electrode polarization at lower frequencies. Thus, the observed dielectric dispersion at higher frequencies cannot reflect the electrode polarization. Instead, an interfacial relaxation process may account for this effect. As considered in previous studies [29,30,52], the dispersed nanoparticles can trap and carry the free charge, leading to the formation of an electric double layer (EDL) on the nanoparticle surfaces. Thus, the EDL polarization may result in the relaxation process reflected in the observed dispersion. This relaxation process is usually described by the Schwarz model of EDL polarization exhibiting a Debye-like behavior as shown elsewhere [30]. The colossal permittivity values in Fig. 2 indicate that in addition to the free charge in the oil, another external charge resulting from the MNF preparation procedure (residual salts, oleate ions, ammonia ions) contributes to the EDL formation. Thus, the polarization of EDLs in MNF may be viewed as local virtual dipoles contributing to the net MNF polarization to a large extent. As the EDL mobility decreases with decreasing temperature (thermal energy), the onset of the dispersion shifts from about 100 Hz at 383 K to 1 Hz at 253 K. The related relaxation time then follows the well-known Arrhenius behavior [29].

One can also notice that in addition to the shift to the lower frequencies, the occurring plateau [real permittivity of a relaxed system at low frequencies, Fig. 2(a)] decreases in magnitude with decreasing temperature. This suggests a development of smaller virtual dipoles in EDLs due to

the restricted charge mobility and polarization conditions in the colder and more viscous oil. The EDL polarization is especially minimal at temperatures of 243 and 233 K, when the oil is supposed to undergo gelation and solidification. In this case, the resulting permittivity does not increase as steeply with decreasing frequency as it does at higher temperatures. Instead, a small dispersion is observed between 10 and 0.1 Hz, as seen from an enlarged view in Fig. 2(b). There, one can see a tendency to form a plateau with permittivity values around 20. The greater increase in permittivity at lower frequencies is ascribed to the electrode polarization.

The liquid-solid phase transition of MNF is confirmed by thermomagnetic measurements. In Fig. 3, we present the temperature-dependent magnetization measured in the ZFC and FC regimes in an external magnetic field of 0.01 T. The obtained profiles reflect a typical behavior of superparamagnetic nanoparticles dispersed in a liquid carrier. The ZFC shoulder around 50 K points out the

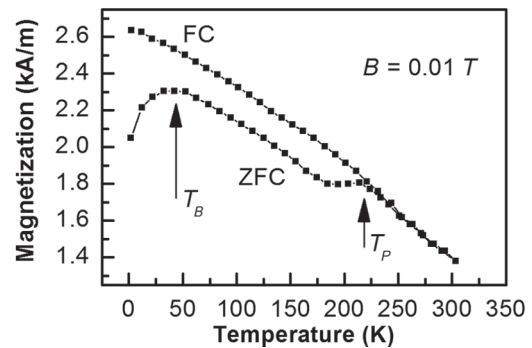


FIG. 3. Temperature-dependent magnetization of MNF measured in ZFC and FC regimes.

area of blocking temperatures T_B . On the other hand, the ZFC maximum at 225 K is associated with the liquid-solid phase transition, and therefore, is ascribed to the freezing of the transformer oil. This finding supports the above explanation of the dielectric response at 243 and 233 K, as it is known that before reaching the freezing point, the oil undergoes gelation.

In the presence of the dc bias voltage, the nature of the frequency-dependent dielectric response of MNF changes markedly. The effect of various dc voltage levels (from 10 to 40 V) on the real permittivity spectrum measured at 233 K is shown in Fig. 4. As the graphs indicate, the positive permittivity drops to negative values below 0.1 Hz for each voltage level. In the negative region, the permittivity

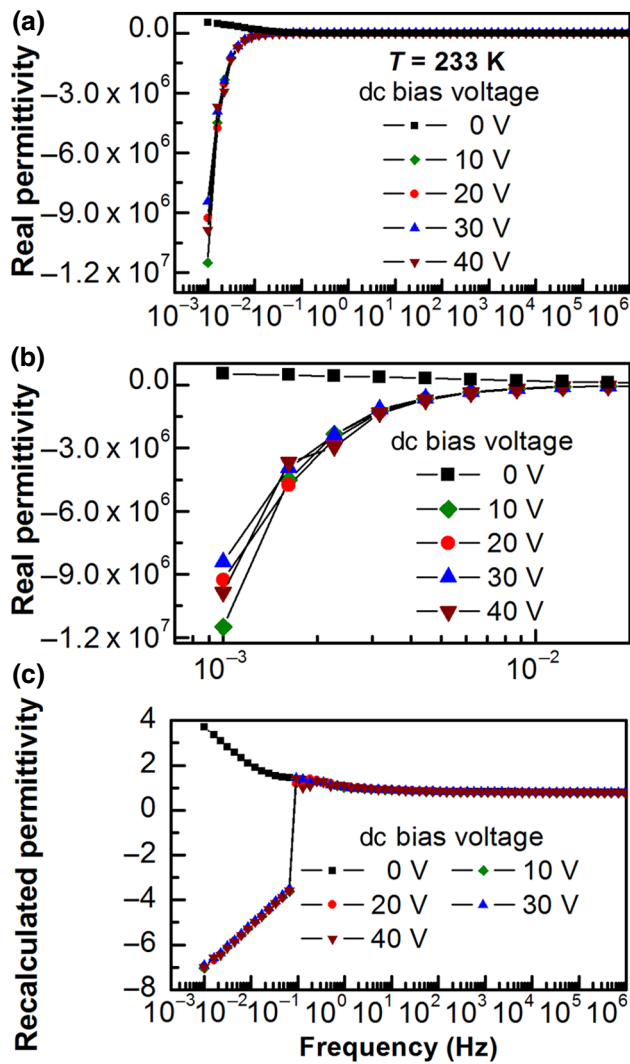


FIG. 4. dc bias voltage influence on the real permittivity spectrum of MNF at 233 K. (a) Whole spectrum with a linear vertical scale. (b) Low-frequency detail on the negative permittivity. (c) Whole spectrum with a base 10 logarithmic vertical scale. The real permittivity values are recalculated according to $\text{sgn}(\epsilon) \times \log[\text{sgn}(\epsilon) \times \epsilon]$.

reaches values up to -10^7 . The maximum value reached at the lowest frequency (1 mHz) varies with the dc voltage level, however, without any logical order, as is seen from the low-frequency detail in Fig. 4(b). As the NP values span a broad range, it is convenient to present the data in a logarithmic scale. To also allow such a presentation for negative values, the measured permittivity data are first converted to positive values by their multiplication with a signum (sgn) function of the measured permittivity data. Subsequently, a common logarithm is calculated from the given positive values. The obtained logarithms are finally multiplied by the signum (sgn) function of the measured permittivity. Thus, the results calculated according to the described formula $\text{sgn}(\epsilon) \times \log[\text{sgn}(\epsilon) \times \epsilon]$ are presented in Fig. 4(c). In this way, one can clearly see that there is a critical frequency at which the positive permittivity abruptly switches to negative values. At a temperature of 233 K, this frequency is 0.1 Hz and it is independent of the dc voltage level. By investigating the dc bias effect on the dielectric response at higher temperatures (283 and 333 K), we find that both the critical frequency and NP reach higher values. In addition, the NP values increase with increasing dc voltage (Fig. 5). In the case of 283 K, the NP at the lowest frequency (1 mHz) in the presence of 10 V is -2.5×10^8 , while under 40 V, the NP increases to -6×10^8 [Fig. 5(b)]. Concerning the critical frequency at 283 K, one can see from the logarithmically recalculated permittivity graph [Fig. 5(c)] that there is not a fixed value. Instead, a few fluctuations between positive and negative permittivity values are detected before stable NP values are measured at lower frequencies. Stable NP values are below 1 Hz for 10 and 30 V, below 2.55 Hz for 20 V, and below 10 Hz for 40 V.

At 333 K, the NP at the lowest frequency again increases by an order of magnitude (Fig. 6). In this case, the NP values range from -3.2×10^9 to -4.7×10^9 under the action of 10 and 40 V, respectively [Fig. 6(b)]. As is seen from Fig. 6(c), the critical frequency is no longer stable and the transition to NP exhibits even more pronounced fluctuations. For the applied dc voltage of 20 V, these fluctuations range from 14 to 0.35 Hz.

Thus, to compare the temperature effect on the broadband dielectric response of MNF in the absence and presence of the dc bias voltage, we plot the logarithmic permittivity values at various temperatures in zero and maximum dc voltages, as depicted in Fig. 7. In zero dc bias voltage, the permittivity spectrum exhibits positive values shifting toward higher frequencies with increasing temperature (as described above). Under the applied dc voltage (40 V), the permittivity spectra follow those measured in zero dc bias voltage only up to the critical frequency, below which the positive values switch to negative values. This critical sign-switching frequency is stable at 233 K. At higher temperatures, it occurs at higher frequencies with noticeable fluctuations between positive and

negative permittivity values. On the other hand, the magnitudes of the stable NP values increase with increasing temperature.

Before analyzing the results, it is worth noting that the presented permittivity sign switching to NP is detected by the two independent devices (Novocontrol Alpha-A spectrometer and HIOKI IM3533 LCR meter). Due to the wide dissipation factor (from 10^{-5} to 10^4) and impedance (from 0.01 to $10^{14} \Omega$) measuring range, and the accuracy in relative impedance and dissipation factor of $< 3 \times 10^{-5}$ (as stated by the Alpha-A producer), we do not ascribe the interpretation of the NP to any experimental error, as the measured values are far from the range and sensitivity

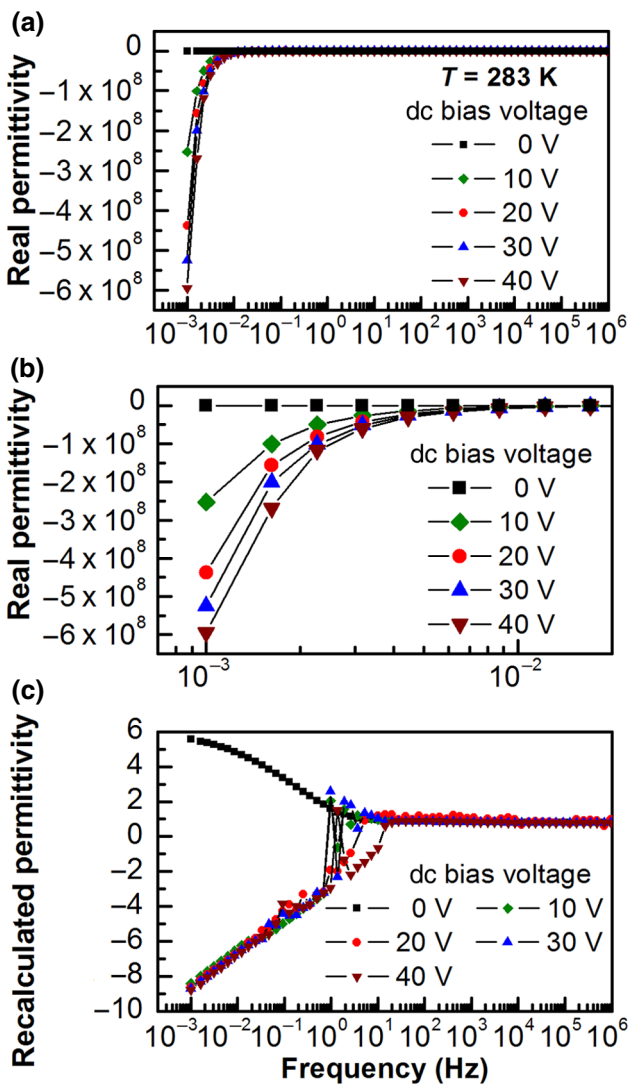


FIG. 5. dc bias voltage effect on the real permittivity spectrum of MNF at 283 K. (a) Whole spectrum with a linear vertical scale. (b) Low-frequency detail on the negative permittivity. (c) Whole spectrum with a base 10 logarithmic vertical scale. The real permittivity values are recalculated according to $\text{sgn}(\epsilon) \times \log[\text{sgn}(\epsilon) \times \epsilon]$.

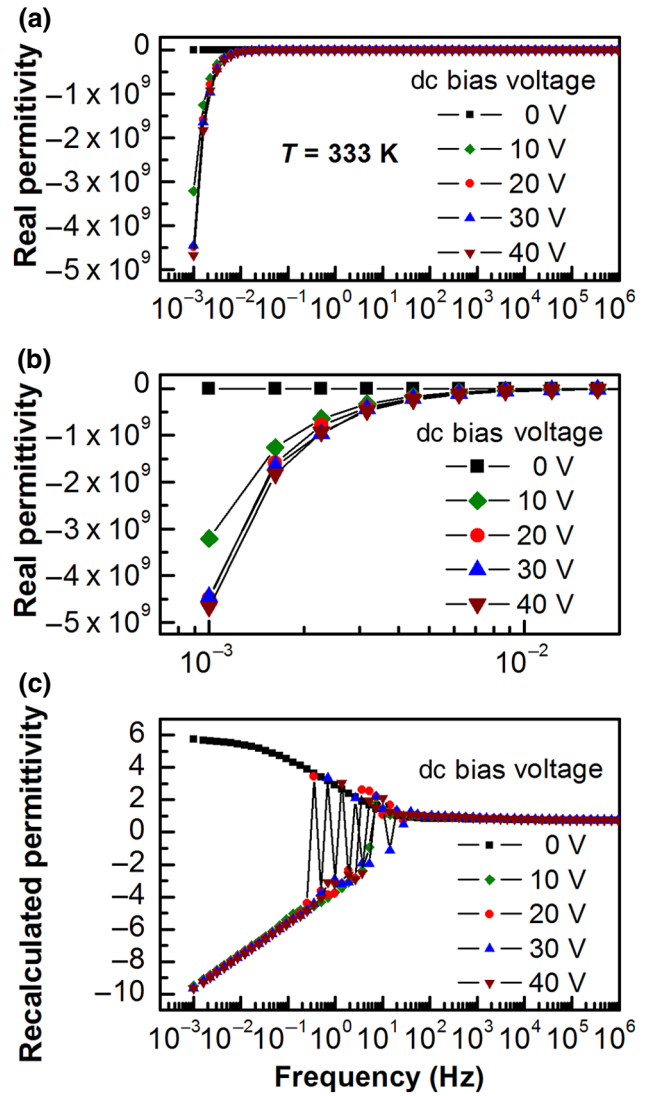


FIG. 6. dc bias voltage effect on the real permittivity spectrum of MNF at 333 K. (a) Whole spectrum with a linear vertical scale. (b) Low-frequency detail on the negative permittivity. (c) Whole spectrum with a base 10 logarithmic vertical scale. The real permittivity values are recalculated according to $\text{sgn}(\epsilon) \times \log[\text{sgn}(\epsilon) \times \epsilon]$.

limits. However, to understand the presented NP results, one has to realize the principle of how the impedance analyzer measures the complex current. When a voltage V_0 with a fixed frequency $\omega/2\pi$ is applied to the sample capacitor, it causes a current I_0 in the sample with the same frequency, but with a phase shift described by the phase angle φ . The time dependent voltage $V(t)$ and current $I(t)$ are given as

$$V(t) = V_0 \cos(\omega t) = \text{Re}[V^* \exp(i\omega t)], \quad (2)$$

$$I(t) = I_0 \cos(\omega t + \varphi) = \text{Re}[I^* \exp(i\omega t)], \quad (3)$$

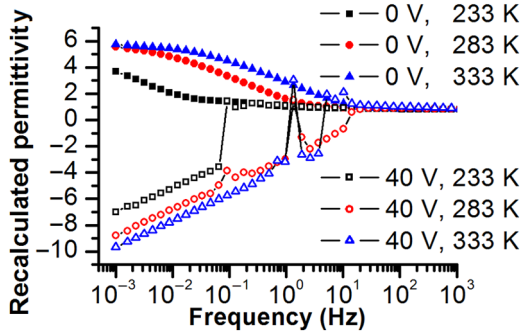


FIG. 7. Comparison of the temperature effect on the common logarithm of the real permittivity of a magnetic nanofluid in the presence of zero and 40-V dc bias voltages. The real permittivity values are recalculated according to $\text{sgn}(\epsilon) \times \log[\text{sgn}(\epsilon) \times \epsilon]$.

where $V^* = V_0$, $I^* = I' + iI''$, $I_0 = \sqrt{I'^2 + I''^2}$, and $\tan(\varphi) = I''/I'$, with I'' and I' denoting the imaginary and real parts of the complex current, respectively. Then, for a material with a linear electromagnetic response, the measured complex impedance is given as follows:

$$Z^*(\omega) = Z' + iZ'' = \frac{V^*}{I^*} = \frac{V_0}{I_0}(\cos \varphi - i \sin \varphi). \quad (4)$$

The complex impedance is connected with the complex permittivity according to the relation

$$\begin{aligned} \epsilon^*(\omega) &= \epsilon' - i\epsilon'' = \frac{1}{i\omega C_0} \cdot \frac{1}{Z^*(\omega)} \\ &= \frac{I_0}{i\omega C_0 V_0} (\cos \varphi + i \sin \varphi), \end{aligned} \quad (5)$$

where C_0 is the geometric capacitance of the empty sample holder. It is, therefore, clear that the phase of the complex current compared to the input voltage is responsible for the complex component. Then, if $\varphi > \pi$, $\sin \varphi$ will be negative, leading to the interpretation of NP. This happens when the conductivity of the studied sample increases.

The increases in electric conductivity of MNF and the associated NP behavior stem from the particle assembly formation induced by the dc and low-frequency electric field [31,32]. Due to the dielectric contrast between the MNP and transformer oil (the oil's permittivity is 2 and the magnetite particles reach permittivity values up to 81), the MNP get preferably polarized by the strong dc field. Subsequently, the induced dipole-dipole interaction and dielectrophoretic forces result in MNP aggregation leading to a percolative state. This assumption is based on the general principles of nanoparticle interaction in an electric field. Generally, the polarized nanoparticles with some shape anisotropy (not a perfect sphere) may experience a torque as a result of the electric force. On the other hand, the nanoparticles with induced electric dipoles

move toward the electric field gradient (dielectrophoresis) and build up the assembly. To form the assemblies, the induced dipolar attraction between neighboring nanoparticles must dominate over the nanoparticle Brownian motion (the basic principles of the colloidal nanoparticle interaction in an electric field under various conditions may be found in Refs. [53,54]). This aggregation in the studied MNF sample in the dc and low-frequency electric field (below 1 Hz) has been documented [31]. However, it seems that the electric field-induced nanoparticle aggregation alone is not enough to induce the apparent negative-permittivity state. If this was sufficient, then one would be able to measure negative permittivity even in the external magnetic field in which the particle assembly is more intuitively formed. However, this is not the case, as we showed in Ref. [29]. The polarization of the surfactant stabilization layers and their overlap seem to be crucial for the formation of conduction paths along the particle assembly. It is known that the mobile charges, such as those in an EDL, also respond to the applied electric field, as reflected in the relaxation maximum (Fig. 2). Then, when the aggregation and percolative state is reached, the EDL regions have higher probability to overlap, creating a high conductivity path. Thus, the free charge can travel along the conductive path. This means that when the magnetic nanofluid reaches the percolative state, the reactance (imaginary impedance) becomes positive and exhibits an inductive character. Therefore, the transition from capacitive to inductive reactance near the percolation threshold is a key factor triggering the detection of NP, as the reactance determines the real permittivity [46]:

$$\epsilon' = \frac{1}{\omega C_0} \left(\frac{-Z''}{Z'^2 + Z''^2} \right). \quad (6)$$

From Eq. (6), it follows that the positive permittivity is attributed to the capacitive character ($Z'' < 0$) and the NP results from the inductive character ($Z'' > 0$). Other reasons for the NP in our study, such as an electrode-related artifact, can be ruled out because, in addition to the stainless-steel capacitor, the dc bias-assisted NP is also detected in a brass cylindrical capacitor and a plate capacitor with ITO layers. Thus, the above presented dc bias-induced apparent NP can be considered as an intrinsic property of the nanoparticle assembly (percolation) formation between the electrodes.

A few factors are responsible for the increasing NP with increasing temperature (Fig. 7). First of all, it is known that the free charge mobility and electrical conductivity in colloidal systems increase with increasing temperature [29]. In addition, the degree of EDL polarizability also increases. It should also be mentioned that both the free charge mobility and EDL polarizability are functions of the carrier liquid viscosity, which decreases with increasing temperature. It is intuitive that the lower the viscosity of

the carrier liquid, the easier and more effective the particle assembly and percolative paths formation. Therefore, the charge mobility and conductivity reasoning are reasonable, especially when comparing the NP of nanofluid in the jelly state (233 K) and in a low viscous state (333 K). Clearly, the higher conductivity at higher temperatures allows the flow of the higher electric current through the sample at a particular dc bias voltage, leading to the higher NP. From Figs. 5(b) and 6(b), it is evident that at 283 and 333 K, the NP increases with increasing dc bias voltage just as a result of the increasing electric current.

The particle assemblies with stable conductive paths are effective even at higher temperatures, as it can be shown that the electrostatic energy of a polarized particle is stronger than the thermal energy acting against the assembling. The parameter α comprising the ratio of the two energies is defined as $pE/k_B T$, with p denoting the effective dipole moment given by the following relation [55]:

$$p = 4\pi \varepsilon_m \left(\frac{\varepsilon_p - \varepsilon_m}{\varepsilon_p + 2\varepsilon_m} \right) R^3 E, \quad (7)$$

where E is the electric field intensity, R is the particle radius, and ε_p and ε_m are the relative permittivities of the particle and the liquid medium, respectively. When considering the limiting case of the highest temperature and the lowest dc electric field in the experiment, the substitution of the relevant values ($T = 333$ K, $E = 2941$ V/m, $R = 10.55$ nm, ε_p of the powder magnetite is reported to range from 34 to 81, $\varepsilon_m = 2$) yields $\alpha \approx 50\,000$. Therefore, even at the highest temperature and the lowest field intensity, the electrostatic energy is greater than the thermal energy approximately by a factor of 50 000. This suggests the presence of stable clusters acting as the conductive paths in the dc field. It is also assumed that the stable particle assembly in the cylindrical capacitor is maintained due to the absence of intensive electrohydrodynamics, which would appear in a nonhomogenous electric field.

The fact that the apparent NP occurs at the low frequencies reflects the stability of the formed clusters and their conductive paths under the low-frequency conditions. While the above stated stability reasoning holds for the dc electric field, the superimposed ac component may constitute a dynamic perturbation in the conductive paths. Apparently, at low enough frequencies, there is a sufficiently long period for the formation of the conducting trees along the particle clusters. The electric charges at the particle interfaces (EDL) are under favorable conditions to be in phase with the ac voltage and to overlap, thus forming the conductive paths, which lead to the apparent NP. Moreover, as confirmed by a neutron scattering experiment [31], the ac field itself with frequencies below 1 Hz induces the particle assemblies, and therefore, the low-frequency ac voltage supports the assembly formation in the dc field. On the other hand, when the frequency approaches the

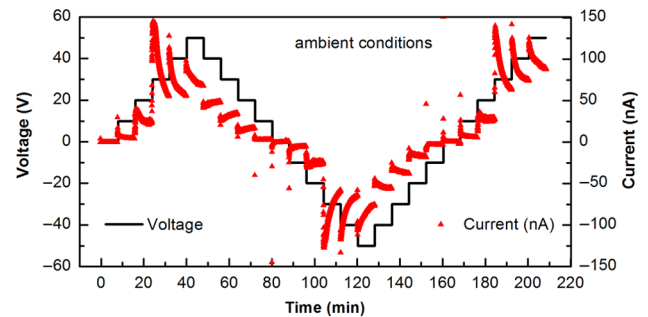


FIG. 8. The time-dependent transient electric current flowing through the magnetic nanofluid at various voltages.

EDL relaxation frequency, the interfacial charges undergo intensive dynamics while responding to the ac voltage. This is believed to disrupt the integrity of the conductive paths along the particle assemblies. The proposed explanation is supported by the fact that the critical frequencies at which the positive permittivity switches to NP (Fig. 7) are approximately consistent with the relaxation frequencies in the absence of the dc field [Fig. 2(d)]. One can see that at 233 K, the relaxation maximum [Fig. 2(d)] and the NP (Fig. 4) occur around 0.1 Hz, while at 283 and 333 K, these effects start to occur around 10 Hz (Figs. 5 and 6). The stable critical frequency and the abrupt transition to NP at 233 K [Fig. 4(c)] is associated with the jelly phase of the oil. Once the percolative threshold is achieved, the conductive paths stay fixed in this phase. The fluctuations in the transition to NP at 283 and 333 K [Figs. 5(c) and 6(c)] reflect the unstable conductive paths in the frequency range from 0.35 to 14 Hz. This is again in good agreement with the neutron scattering results in the ac electric field, which reveals the particle clusters below 0.8 Hz [31].

Finally, when considering the electric current flowing through the sample as an important factor in determining the apparent NP, it is valuable to present its behavior under various dc voltage levels. In Fig. 8, we demonstrate the time-dependent electric current at various voltages, which is measured at 8-min time intervals at room temperature. For the steplike increasing voltage, the transient electric current follows a typical charging behavior with decreasing values in time and a tendency to reach a stabilized value. The decaying current under the constant voltage is associated with the charge settling response, which resembles a charging current. In this case, upon application of the increased voltage, the space charge drifts to the electrode with an opposite polarity. The ion impurities and the nanoparticles with the uncompensated surface charge may create EDLs near the electrodes. Then, the absorption current diminishes and the leakage current is maintained by the electron charge transfer between the electrodes and the nanofluid. On the other hand, for the steplike decreasing voltage, the transient current exhibits a discharging behavior. The discharging current represents the release of the

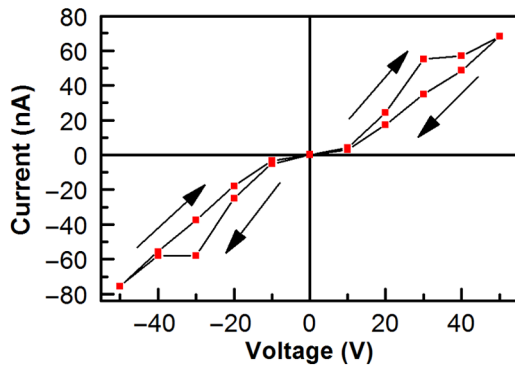


FIG. 9. The I - V characteristics measured on the magnetic nanofluid. The presented data points are taken in the eighth minute after the application of the particular voltage. The upper arrows, pointing from the left to the right, indicate the curves measured in the increasing voltage regime, while the lower arrows, pointing from the right to the left, indicate the curves measured in the decreasing voltage regime.

accumulated charge near the electrode with the subsequent increase in the electrode potential.

When plotting the voltage dependence of the leakage current taken at the eighth minute after the application of a particular voltage, one gets the I - V characteristics presented in Fig. 9. It can be seen that the characteristics exhibit a hysteresislike behavior, as the current values measured in the increasing voltage regime (the upper curve) do not match with those measured in the decreasing regime (the lower curve). Thus, an I - V loop is formed under both positive and negative voltages. The nonlinear character in the upper curves reflects the changes in the MNF structure and formation of conductive paths via the described EDL overlap in the particle clusters. A remarkable increase in current (conductivity) is observed, especially for 20 and 30 V, which is the result of the well-formed conductive paths. The further decrease in the I - V slope at higher voltages can be attributed to the accumulated charge near the electrodes, which lowers the electrode potential. When measuring the current in the decreasing voltage regime, one can observe a quasilinear behavior. This is the result of the proportional deceleration of the charge drift due to the decreasing voltage. As the current returns back to zero at zero voltage, one can conclude that there is no energy storage or capacitive effect. Thus, the conductive paths formation in the increasing voltage is a reversible process and can be considered as a triggering factor of the reported apparent NP.

IV. CONCLUSIONS

We show that the transformer oil-based magnetic nanofluid can exhibit a dc bias tunable apparent negative permittivity behavior at low frequencies. This effect is a result of the particle clustering and the interface charge

overlap in the applied electric field. Due to the created percolative conductive paths, the nanofluid undergoes transition from capacitive to inductive reactance. This mechanism is feasible at a low-frequency electric field without dynamic perturbations. The negative permittivity increases with increasing temperature. The increased conductivity triggering the observed negative permittivity is reflected in the increased I - V slope. From an application point of view, the measurement of apparent negative permittivity in colloidal nanoparticle systems can be used as an indication method of the particle assembly and percolation. The magnetic nanofluid with tunable negative permittivity can find applications in the field of sensors based on the permittivity change. Thus, besides the attractive magneto-dielectric properties, the electric field-induced permittivity sign switching may open an alternate avenue for research and applications of magnetic nanofluids.

ACKNOWLEDGMENT

This work was supported by the Slovak Academy of Sciences and Ministry of Education in the framework of projects VEGA Grants No. 2/0141/16, No. 2/0093/16, No. 2/0016/17, and No. 1/0340/18, Ministry of Education Agency for structural funds of EU Projects ITMS Grants No. 26220220186 and No. 26220120055, COST Grant No. CA15119 NANOUPTAKE, and Slovak Research and Development Agency under Grants No. APVV-15-0453, No. APVV-15-0438, and No. APVV-17-0372.

The manuscript was written with contributions from all authors. All authors have given approval to the final version of the manuscript.

- [1] T. J. Lewis, Nanometric dielectrics, *IEEE Trans. Dielectr. Electr. Insul.* **1**, 812 (1994).
- [2] M. F. Frechette, M. L. Trudeau, H. D. Alamdar, and S. Boily, Introductory remarks on nanodielectrics, *IEEE Trans. Dielectr. Electr. Insul.* **11**, 808 (2004).
- [3] Y. Cao, P. C. Irwin, and K. Younsi, The future of nanodielectrics in the electrical power industry, *IEEE Trans. Dielectr. Electr. Insul.* **11**, 797 (2004).
- [4] S. Siddabattuni, T. P. Schuman, and F. Dogan, Dielectric properties of polymer-particle nanocomposites influenced by electronic nature of filler surfaces, *ACS Appl. Mater. Interfaces* **5**, 1917 (2013).
- [5] T. Tanaka, G. C. Montanari, and R. Mulhaupt, Polymer nanocomposites as dielectrics and electrical insulation—perspectives for processing technologies, material characterization and future applications, *IEEE Trans. Dielectr. Electr. Insul.* **11**, 763 (2004).
- [6] T. Tanaka, Dielectric nanocomposites with insulating properties, *IEEE Trans. Dielectr. Electr. Insul.* **12**, 914 (2005).
- [7] R. Bartnikas, *Electrical Insulating Liquids* (Astm Int'l, Philadelphia, PA, 1994).

- [8] R. Taylor, S. Coulombe, T. Otanicar, P. Phelan, A. Gunawan, W. Lv, G. Rosengarten, R. Prasher, and H. Tyagi, Small particles, big impacts: A review of the diverse applications of nanofluids, *J. Appl. Phys.* **113**, 011301 (2013).
- [9] Y. Z. Lv, Y. Zhou, C. R. Li, Q. Wang, and B. Qi, Recent progress in nanofluids based on transformer oil: Preparation and electrical insulation properties, *IEEE Electr. Insul. Mag.* **30**, 23 (2014).
- [10] W. Yu, H. Xie, W. Yu, and H. Xie, A review on nanofluids: Preparation, stability mechanisms, and applications, *J. Nanomater.* **2012**, e435873 (2011).
- [11] B. Ma and D. Banerjee, *A Review of Nanofluid Synthesis, Advances in Nanomaterials* (Springer, Cham, 2018), pp. 135–176.
- [12] J. A. Esfahani, M. R. Safaei, M. Goharimanesh, L. R. de Oliveira, M. Goodarzi, S. Shamshirband, and E. P. B. Filho, Comparison of experimental data, modelling and non-linear regression on transport properties of mineral oil based nanofluids, *Powder Technol.* **317**, 458 (2017).
- [13] H. Taherian, J. L. Alvarado, and E. M. Languri, Enhanced thermophysical properties of multiwalled carbon nanotubes based nanofluids. Part 1: Critical review, *Renew. Sustain. Energy Rev.* **82**, 4326 (2018).
- [14] S. Ab Ghani, N. A. Muhamad, Z. Z. Noorden, H. Zainuddin, N. Abu Bakar, and M. A. Talib, Methods for improving the workability of natural ester insulating oils in power transformer applications: A review, *Electr. Power Syst. Res.* **163**, 655 (2017).
- [15] M. Rafiq, Y. Lv, and C. Li, A review on properties, opportunities, and challenges of transformer oil-based nanofluids, *J. Nanomater.* **2016**, e8371560 (2016).
- [16] H. Kojima, T. Kondo, M. Hanai, and N. Hayakawa, Improvement mechanism of AC breakdown voltage of insulating oil with dispersed nanoparticles, *Electron. Commun. Jpn.* **100**, 69 (2017).
- [17] J. Taha-Tijerina, T. N. Narayanan, G. Gao, M. Rohde, D. A. Tsentalovich, M. Pasquali, and P. M. Ajayan, Electrically insulating thermal nano-oils using 2D fillers, *ACS Nano* **6**, 1214 (2012).
- [18] S. Odenbach, *Colloidal Magnetic Fluids: Basics, Development and Application of Ferrofluids* (Springer-Verlag, Berlin Heidelberg, 2009).
- [19] I. Nkurikiyimfura, Y. Wang, and Z. Pan, Heat transfer enhancement by magnetic nanofluids—A review, *Renew. Sustain. Energy Rev.* **21**, 543 (2013).
- [20] V. Chaudhary, Z. Wang, A. Ray, I. Sridhar, and R. V. Ramanujan, Self pumping magnetic cooling, *J. Phys. Appl. Phys.* **50**, 03LT03 (2017).
- [21] A. Lange and S. Odenbach, Patterns of thermomagnetic convection in magnetic fluids subjected to spatially modulated magnetic fields, *Phys. Rev. E* **83**, 066305 (2011).
- [22] V. Segal, A. Hjortsberg, A. Rabinovich, D. Natrass, and K. Raj, AC (60 Hz) and Impulse Breakdown Strength of a Colloidal Fluid Based on Transformer Oil and Magnetite Nanoparticles, Conference Record of the 1998 IEEE International Symposium on Electrical Insulation 1998, 619 (1998).
- [23] J. C. Lee, H. S. Seo, and Y. J. Kim, The increased dielectric breakdown voltage of transformer oil-based nanofluids by an external magnetic field, *Int. J. Therm. Sci.* **62**, 29 (2012).
- [24] Y. Lv, M. Rafiq, C. Li, and B. Shan, Study of dielectric breakdown performance of transformer oil based magnetic nanofluids, *Energies* **10**, 1025 (2017).
- [25] J. G. Hwang, M. Zahn, F. M. O'Sullivan, L. A. A. Petersson, O. Hjortstam, and R. Liu, Effects of nanoparticle charging on streamer development in transformer oil-based nanofluids, *J. Appl. Phys.* **107**, 014310 (2010).
- [26] J. Velasco, R. Frascella, R. Albaracín, J. C. Burgos, M. Dong, M. Ren, and L. Yang, Comparison of positive streamers in liquid dielectrics with and without nanoparticles simulated with finite-element software, *Energies* **11**, 361 (2018).
- [27] J. Miao, M. Dong, M. Ren, X. Wu, L. Shen, and H. Wang, Effect of nanoparticle polarization on relative permittivity of transformer oil-based nanofluids, *J. Appl. Phys.* **113**, 204103 (2013).
- [28] N. A. Yusuf, J. Shobaki, H. Abu-Safia, and I. Abu-Aljarayesh, Magneto-dielectric anisotropy in magnetic fluids determined from magneto-optical measurements, *J. Magn. Magn. Mater.* **149**, 373 (1995).
- [29] M. Rajnak, B. Dolnik, J. Kurimsky, R. Cimbala, P. Kopcansky, and M. Timko, Electrode polarization and unusual magnetodielectric effect in a transformer oil-based magnetic nanofluid thin layer, *J. Chem. Phys.* **146**, 014704 (2017).
- [30] M. Rajnak, J. Kurimsky, B. Dolnik, P. Kopcansky, N. Tomasovicova, E. A. Taculescu-Moaca, and M. Timko, Dielectric-spectroscopy approach to ferrofluid nanoparticle clustering induced by an external electric field, *Phys. Rev. E* **90**, 032310 (2014).
- [31] M. Rajnak, V. I. Petrenko, M. V. Avdeev, O. I. Ivankov, A. Feoktystov, B. Dolnik, J. Kurimsky, P. Kopcansky, and M. Timko, Direct observation of electric field induced pattern formation and particle aggregation in ferrofluids, *Appl. Phys. Lett.* **107**, 073108 (2015).
- [32] R. Cimbala, J. Kurimský, M. Rajnák, K. Paulovičová, M. Timko, P. Kopčanský, M. Kolcun, M. Kosterec, S. Bucko, and M. Kurimská, Magnetic fluid droplet deformation in electrostatic field, *J. Electrostat.* **88**, 55 (2017).
- [33] M. Rajnak, M. Timko, P. Kopcansky, K. Paulovicova, J. Tothova, J. Kurimsky, B. Dolnik, R. Cimbala, M. V. Avdeev, V. I. Petrenko, and A. Feoktystov, Structure and viscosity of a transformer oil-based ferrofluid under an external electric field, *J. Magn. Magn. Mater.* **431**, 99 (2017).
- [34] C. W. Chu, F. Chen, J. Shulman, S. Tsui, Y. Y. Xue, W. Wen, and P. Sheng, A negative dielectric constant in nano-particle materials under an electric field at very low frequencies, *Int. Soc. Opt. Photonics* **5932**, 59320X (2005).
- [35] F. Chen, J. Shulman, S. Tsui, Y. Y. Xue, W. Wen, P. Sheng, and C. W. Chu, Field-induced giant static dielectric constant in nano-particle aggregates at room temperature, *Philos. Mag.* **86**, 2393 (2006).
- [36] S. H. Zaidi and A. K. Jonscher, Spectroscopy of delayed electronic transitions in GaAs Schottky diodes, *Semicond. Sci. Technol.* **2**, 587 (1987).
- [37] F. Hajbolouri, B. Andreaus, G. Scherer, and A. Wokaun, CO tolerance of commercial Pt and PtRu gas diffusion electrodes in polymer electrolyte fuel cells, *Fuel Cells* **4**, 160 (2004).

- [38] H. G. Çetinkaya, S. Alialy, S. Altindal, A. Kaya, and I. Uslu, Investigation of negative dielectric constant in Au/1% graphene (GP) Doped-Ca_{1.9}Pr_{0.1}Co₄O_x-n-Si structures at forward biases using impedance spectroscopy analysis, *J. Mater. Sci. Mater. Electron.* **26**, 3186 (2015).
- [39] X. Zhang, X. Yan, Q. He, H. Wei, J. Long, J. Guo, H. Gu, J. Yu, J. Liu, D. Ding, L. Sun, S. Wei, and Z. Guo, Electrically conductive polypropylene nanocomposites with negative permittivity at low carbon nanotube loading levels, *ACS Appl. Mater. Interfaces* **7**, 6125 (2015).
- [40] H. Kavas, M. Günay, A. Baykal, M. S. Toprak, H. Sozeri, and B. Aktaş, Negative permittivity of polyaniline-Fe₃O₄ nanocomposite, *J. Inorg. Organomet. Polym. Mater.* **23**, 306 (2013).
- [41] H. Gu, J. Guo, S. Wei, and Z. Guo, Polyaniline nanocomposites with negative permittivity, *J. Appl. Polym. Sci.* **130**, 2238 (2013).
- [42] Y. F. Hou, W. L. Li, T. D. Zhang, Y. Yu, R. L. Han, and W. D. Fei, Negative capacitance in BaTiO₃/BiFeO₃ bilayer capacitors, *ACS Appl. Mater. Interfaces* **8**, 22354 (2016).
- [43] Y. J. Kim, M. H. Park, Y. H. Lee, H. J. Kim, W. Jeon, T. Moon, K. Do Kim, D. S. Jeong, H. Yamada, and C. S. Hwang, Frustration of negative capacitance in Al₂O₃/BaTiO₃ bilayer structure, *Sci. Rep.* **6**, 19039 (2016).
- [44] D. R. Smith, W. J. Padilla, D. C. Vier, S. C. Nemat-Nasser, and S. Schultz, Composite Medium with Simultaneously Negative Permeability and Permittivity, *Phys. Rev. Lett.* **84**, 4184 (2000).
- [45] K. Sun, R. H. Fan, Z. D. Zhang, K. L. Yan, X. H. Zhang, P. T. Xie, M. X. Yu, and S. B. Pan, The tunable negative permittivity and negative permeability of percolative Fe/Al₂O₃ composites in radio frequency range, *Appl. Phys. Lett.* **106**, 172902 (2015).
- [46] K. Sun, R. Fan, Y. Yin, J. Guo, X. Li, Y. Lei, L. An, C. Cheng, and Z. Guo, Tunable negative permittivity with fano-like resonance and magnetic property in percolative silver/yttrium iron garnet nanocomposites, *J. Phys. Chem. C* **121**, 7564 (2017).
- [47] J. Krupka, B. Salski, P. Kopyst, and W. Gwarek, Electrodynamic study of YIG filters and resonators, *Sci. Rep.* **6**, 34739 (2016).
- [48] J. Krupka, J. Wosik, C. Jastrzębski, T. Ciuk, J. Mazierska, and M. Zdrojek, Complex conductivity of YBCO films in normal and superconducting states probed by microwave measurements, *IEEE Trans. Appl. Supercond.* **23**, 1501011 (2013).
- [49] V. M. Shalaev, Optical negative-index metamaterials, *Nat. Photonics* **1**, 41 (2007).
- [50] L. Vékás, D. Bica, and M. V. Avdeev, Magnetic nanoparticles and concentrated magnetic nanofluids: Synthesis, properties and some applications, *China Particuology* **5**, 43 (2017).
- [51] R. J. Klein, S. Zhang, S. Dou, B. H. Jones, R. H. Colby, and J. Runt, Modeling electrode polarization in dielectric spectroscopy: Ion mobility and mobile ion concentration of single-ion polymer electrolytes, *J. Chem. Phys.* **124**, 144903 (2006).
- [52] M. Dong, J. Dai, Y. Li, J. Xie, M. Ren, and Z. Dang, Insight into the dielectric response of transformer oil-based nanofluids, *AIP Adv.* **7**, 025307 (2017).
- [53] M. Grzelczak, J. Vermant, E. M. Furst, and L. M. Liz-Marzán, Directed self-assembly of nanoparticles, *ACS Nano* **4**, 3591 (2010).
- [54] E. V. Yakovlev, K. A. Komarov, K. I. Zaytsev, N. P. Kryuchkov, K. I. Koshelev, A. K. Zotov, D. A. Shelestov, V. L. Tolstoguzov, V. N. Kurlov, A. V. Ivlev, and S. O. Yurchenko, Tunable two-dimensional assembly of colloidal particles in rotating electric fields, *Sci. Rep.* **7**, 13727 (2017).
- [55] H. Morgan, and N. G. Green, *AC Electrokinetics: Colloids and Nanoparticles* (Research Studies Press, Baldock, Hertfordshire, England, 2003).